Survey of Whistler-mode Wave Amplitudes and Frequency Spectra in Jupiter's Magnetosphere

Q. Ma[1,2], W. Li[2], X.-J. Zhang[3], N. Kang[1], J. Bortnik[1], M. Qin[2], X.-C. Shen[2], C. J. Meyer-Reed[2], A. V. Artemyev[4], W. S. Kurth[5], G. B. Hospodarsky[5], J. D. Menietti[5], and S. J. Bolton[6]

[1]Department of Atmospheric and Oceanic Sciences, University of California, Los Angeles, California, USA.

[2]Center for Space Physics, Boston University, Boston, Massachusetts, USA.

[3]Department of Physics, University of Texas at Dallas, Richardson, Texas, USA.

[4]Department of Earth, Planetary, and Space Sciences, University of California, Los Angeles, CA, USA

[5]Department of Physics and Astronomy, University of Iowa, Iowa City, Iowa, USA.

[6]Southwest Research Institute, San Antonio, Texas, USA.

Corresponding author: Qianli Ma (qianlima@ucla.edu)

Key Points:

- Intense chorus waves at 0.05-1 equatorial electron gyrofrequencies ($f_{ce,eq}$) are observed at 5.5<M<13 within 20° magnetic latitudes
- Hiss waves from 50 Hz to 0.05 $f_{ce,eq}$ have extended latitudinal coverage up to 50° and exhibit propagation effects
- High latitude (>50°) whistler-mode waves at 0.05-1 $f_{ce,eq}$ are observed in two groups due to different sources

Abstract

We present statistical distributions of whistler-mode chorus and hiss waves at frequencies ranging from the local proton gyrofrequency to the equatorial electron gyrofrequency ($f_{ce,eq}$) in Jupiter's magnetosphere based on Juno measurements. The chorus wave power spectral densities usually follow the $f_{ce,eq}$ variation with major wave power concentrated in the $0.05f_{ce,eq}$–$f_{ce,eq}$ frequency range. The hiss wave frequencies are less dependent on $f_{ce,eq}$ variation than chorus with major power concentrated below $0.05f_{ce,eq}$, showing a separation from chorus at $M<10$. Our survey indicates that chorus waves are mainly observed at $5.5<M<13$ from the magnetic equator to 20° latitude, consistent with local wave generation near the equator and damping effects. The hiss wave powers extend to 50° latitude, suggesting longer wave propagation paths without attenuation. Our survey also includes the whistler-mode waves at high latitudes which may originate from the Io footprint, auroral hiss, or propagating hiss waves reflected to high *M* shells.

Plain Language Summary

Whistler-mode chorus and hiss waves in Jupiter's magnetosphere are major plasma wave modes, characterized by perturbations in electric and magnetic fields at frequencies from the proton gyrofrequency to the electron gyrofrequency. Chorus waves are typically observed at $0.05f_{ce,eq}$ – $f_{ce,eq}$ frequencies ($f_{ce,eq}$ is the electron gyrofrequency at the equator) with coherent wave structures. Chorus waves, generated by hot electrons, could cause electron precipitation into the atmosphere and acceleration in the radiation belt. In contrast, hiss waves are usually incoherent with wave frequencies less dependent on $f_{ce,eq}$ than chorus. Hiss waves have mixed sources and mainly drive energetic electron loss. Using Juno satellite measurements, we analyze the statistical distribution of chorus and hiss waves in Jupiter's magnetosphere. Our survey reveals different latitudinal coverages and statistical properties of chorus and hiss waves, suggesting their different sources and damping effects. Additionally, our survey includes whistler-mode waves at high latitudes, potentially originating from various sources such as the Io footprint at the ionosphere, auroral hiss, or reflection of hiss waves at high *M* shells. The whistler-mode wave distributions from our study provide valuable insights for future modeling of whistler-mode wave sources and energetic electron dynamics in Jupiter's magnetosphere.

1. Introduction

Whistler-mode waves in Jupiter's magnetosphere have recently garnered increased attention due to their pivotal role in shaping energetic electron dynamics in the radiation belts (Horne et al., 2008; Menietti et al., 2023; Woodfield et al., 2014). For comparison, in the Earth's magnetosphere, whistler-mode chorus waves are tyically observed over $0.05–0.5f_{ce,eq}$ and $0.5–1\,f_{ce,eq}$ frequencies outside the plasmapause (Li et al., 2009, 2016; Meredith et al., 2012), where $f_{ce,eq}$ is the electron gyrofrequency at the magnetic equator; hiss waves are observed at 20 Hz – 4 kHz frequencies in the plasmasphere and plumes (Li et al., 2015; Ma et al., 2023). Chorus waves typically exhibit discrete and coherent wave structures (Li et al., 2011; Santolík et al., 2003), and cause plama sheet electron scattering loss and precipitation and radiation belt electron acceleration (Agapitov et al., 2013; Blum et al., 2020; Lorentzen et al., 2001; Thorne et al., 2010, 2013). Hiss waves usually have a broadband and incoherent frequency spectrum and cause energetic electron flux decay in the outer radiation belt (Ma et al., 2016). Whistler-mode waves are suggested to play similar roles in Jupiter's middle magnetosphere (Bhattacharya et al., 2005;

Li et al., 2021; Ma et al., 2020; Shprits et al., 2012; Woodfield et al., 2013), potentially having a significant impact on electron precipitation and acceleration between the orbits of Io and Ganymede. Global wave distributions and detailed wave properties of chorus and hiss are required to evaluate the electron dynamics due to whistler-mode waves in Jupiter's magnetosphere, and model the multi-MeV electron distributions in the radiation belts (e.g., Ma et al., 2021), but the large volume of observations needed to create such global distributions has not been available until recently.

The Juno spacecraft (Bagenal et al., 2017; Bolton et al., 2010) arrived at Jupiter's magnetosphere in July 2016, and has been sampling the low-latitude region at M shells below 15 since May 2019. The M shell is the jovicentric radial distance of the field line at the magnetic equator normalized to the Jupiter's radius (R_J~71,492 km). Previous studies have revealed that whistler-mode waves are commonly observed over $6 < M < 15$ from the equator to 50° magnetic latitudes (Li et al., 2020; Menietti et al., 2016, 2020, 2021, 2023). The detailed wave frequency spectrum, which determines the energy of electron precipitation and acceleration, requires further investigation. The power of chorus and hiss waves is typically characterized by higher and lower frequency ranges normalized to the equatorial electron gyrofrequency ($f/f_{ce,eq}$), respectively. Energetic electron injections may provide free energy for local chorus wave generation in Jupiter's magnetosphere (Xiao et al., 2003; Ma et al., 2024a). Wang et al. (2008) suggested that hiss waves at frequencies below 1 kHz originate from chorus waves at higher M shells, considering the fact that the cyclotron resonance energy for hiss is above 1 MeV. The most recent Juno measurements provide data near the magnetic equator over $M > 5$, fully covering the critical region of major whistler-mode wave activity. In this paper, we present the statistics of whistler-mode wave spectra at different M shells and magnetic latitudes (MagLat) and reveal the distribution and properties of chorus and hiss separately. Our findings provide valuable insights into the generation source, propagation, and damping processes of whistler-mode waves in Jupiter on a global scale.

2. Whistler-mode Wave Observations by the Juno Satellite

We analyze Juno measurements of whistler-mode waves during its first 57 orbits from July 2016 to December 2023. We use the 1-s resolution magnetometer (MAG) data to obtain the background magnetic fields (Connerney et al., 2017) and calculate the local gyrofrequencies of protons ($f_{cp,local}$) and electrons ($f_{ce,local}$). The Waves instrument provides the wave magnetic (B_w) and electric (E_w) power spectral densities at 50 Hz - 20 kHz frequencies and 50 Hz - 40 MHz frequencies, respectively, with a time resolution of 1 s (Kurth et al., 2017). Jupiter's internal magnetic field model JRM-33 (Connerney et al., 2022a) and external current sheet model CON-2020 (Connerney et al., 2020) are used to calculate the M shell and map the measured local magnetic field to the magnetic equator. The $f_{ce,eq}$ is calculated using the ratio of equatorial to local magnetic fields and the observed $f_{ce,local}$.

Figure 1 shows typical whistler-mode wave observations at different regions in Jupiter's magnetosphere. The root-mean-square (RMS) amplitude of wave magnetic field collected at frequencies $f_{cp,local} < f < f_{ce,eq}$ is shown in Figure 1m, over-plotted by the Juno trajectories during different events shown in Figures 1a-l. Within 10° of the magnetic equator (Figure 1a), bursts of whistler-mode waves were observed at frequencies both above and below $0.05f_{ce,eq}$ (white line with black dots). The two-band whistler-mode waves with a gap at ~$0.05f_{ce,eq}$ were most evident when Juno was at $M < 7.6$ after 1600 UT. The frequency spectra of the higher frequency band ($f > 0.05 f_{ce,eq}$) follow the variation of $f_{ce,eq}$, while the lower frequency band ($f < 0.05 f_{ce,eq}$) wave powers remain in a stable frequency range below ~1 kHz. Hereafter, based on these consistent morphological differences, we categorize the waves at $0.05 f_{ce,eq} < f < f_{ce,eq}$ frequencies as chorus and the waves at $f_{cp,local} < f < 0.05 f_{ce,eq}$ as hiss waves. The chorus waves could have discrete elements as shown by Ma et al. (2024a). In addition to the evidence of the wave power gap at $\sim 0.05 f_{ce,eq}$, this categorization aligns with the facts that the waves at higher $f / f_{ce,eq}$ could be locally generated and the lower frequency hiss waves may originate by propagation from a remote source (Wang et al., 2008), and is consistent with the fact that the chorus waves in the Earth's radiation belts are mainly observed at frequencies above $0.05 f_{ce,eq}$ (Li et al., 2016). The different properties of chorus and hiss waves are also supported by the analysis of wave burst mode data (Supporting Information Figures S1-S5).

Over MagLat ~10°–20° (Figure 1c), Juno also observed chorus and hiss waves with a wave power minimum at $\sim 0.05 f_{ce,eq}$ frequency at $M < 9.9$. Compared to the whistler-mode waves observed near the equator (Figure 1a), the wave power spectrograms appear less bursty at higher magnetic latitudes (Figure 1c). Over MagLat ~30°–40° (Figure 1e), the chorus wave powers are significantly reduced compared to the lower latitude measurements, while the hiss wave power intensities are moderate with the majority of power observed between $f_{cp,local}$ and $0.05 f_{ce,eq}$.

The whistler-mode wave power spectrogram at MagLat >50° shows a different feature compared to those observed at lower magnetic latitudes. At MagLat >50° and $M > 12.9$ (Figure 1g), a band of whistler-mode waves was observed with a lower cutoff frequency slightly below $f_{cp,local}$. Juno also observed intense auroral hiss waves (Elliott et al., 2020; Santolík & Gurnett, 2002; Sulaiman et al., 2022) after traveling to the polar region at 0730 UT, where $f_{cp,local} > f_{ce,eq}$. The waves observed before 0730 UT may originate either from the auroral hiss waves propagating obliquely across magnetic field lines to lower *M* shells, or from hiss wave originating from low-latitudes reflected at MagLat~50° away from Jupiter towards higher *M* shells. The auroral hiss waves are generated by the electron beams in Jupiter's polar region (Elliott et al., 2020), while the hiss waves from the low latitudes may be amplified by anisotropic electrons (Chen et al., 2012) or originate from chorus waves at higher *M* shells (Wang et al., 2008). The wave burst data analysis suggests that the Poynting flux direction is away from Jupiter (Supporting Information Figure S4). The full wave polarization properties may be helpful to identify the source of whistler-mode waves at MagLat >50° (as shown in Figure 1g), which cannot be determined from the one-component measurements of wave electric and magnetic fields.

Juno observed whistler-mode waves in the vicinity of perijove at MagLat >50°. Figure 1i shows the wave observation when Juno was close to the Io footprint at the radial distance $R < 1.5$. The variations of plasma waves and particles during this event were analyzed in previous studies (Clark et al., 2020, 2023; Sulaiman et al., 2020; Szalay et al., 2020). At ~0921 UT, Juno observed kinetic Alfven waves at <800 Hz frequencies, electromagnetic ion cyclotron (EMIC) waves at 800 Hz $- f_{\mathrm{cp,local}}$ frequencies, and whistler-mode waves with the majority of power at $f_{cp,local}$– $f_{ce,eq}$ frequencies. The whistler-mode waves related to the Io footprint have a broader spatial extent than the EMIC or kinetic Alfven waves. When Juno was not in conjuction with the Io footprint at $R > 1.5$ (Figure 1k), whistler-mode waves with reduced intensities are observed, comprised of a branch with maximum power at $M{\sim}6$ and ~10 kHz frequency, and another branch over $M > 7$ at frequencies just above $f_{cp,local}$ and below $f_{ce,eq}$.

For the purpose of statistical analysis, we select the whistler-mode waves at $f_{cp,local} < f < f_{ce,eq}$ frequencies by requiring the wave magnetic power spectral density to be at least 3 times higher than the background noise level to ensure a real wave observation. The background noise power at each frequency is obtained as the 20% lowest power on each day. Using this criterion, the selected whistler-mode waves are shown on the bottom panels of each event. By setting $f < f_{ce,eq}$, our method selects the whistler-mode waves originated at the magnetic equator (Figures 1a-f). The EMIC and kinetic Alfven waves are excluded from our database (Figures 1i-l). The Z-mode waves at $M > 5.5$ are excluded because they are mainly observed at high latitudes (Menietti et al., 2020, 2021, 2023) with frequencies higher than $f_{ce,eq}$. The main powers of auroral hiss at the polar region are also excluded where $f_{ce,eq} < f_{cp,local}$ (Figures 1g-h). Since the waves at >50° magnetic latitudes and $R > 2.5$ may be not confined within $f_{cp,local}$–$f_{ce,eq}$ frequencies (Figures 1g-h), their powers may be slightly underestimated. However, these waves exist in a small spatial region (Figure 1m) and may have a different source from the lower latitude whistler-mode waves.

3. Statistical Distribution of Whistler-mode Chorus and Hiss Waves

We average the selected wave powers in every 0.2 wide *M* shell bin, in every 2° MagLat, and at each frequency channel of Waves survey mode data. If whistler-mode waves are not observed, the wave power spectral densities are recorded as 0 and included in averaging. The period of Juno's flyby of Ganymede during PJ-34 is excluded from our dataset, because the magnetic field lines are strongly affected by Ganymede's internal magnetic field and the calculated $f_{ce,eq}$ is not accurate. During the first ~7 years, the Juno Waves instrument collected sufficient number of data samples at 1-s cadence especially at $M < 20$ or $|MagLat| < 40°$, except for the lack of data at $M < 5$ and $|MagLat| < 20°$ (Figure 2c).

Figure 2a shows the wave spectra at different *M* shells for all magnetic latitudes, and Figure 2b shows the root-mean-square (RMS) wave amplitude distribution as a function of *M* shell and |MagLat|. At $|MagLat| < 25°$, whistler-mode waves at $f_{cp,local} < f < f_{ce,eq}$ frequencies are mainly observed at $5.5 < M < 15$. The *M* shell range of whistler-mode waves may correspond to the region where energetic electron injections provide anisotropic fluxes needed for local wave generation (Mauk et al., 1999; Tomás et al., 2004; Ma et al., 2021). The cutoff of whistler-mode wave power at $M{\sim}5.5$ corresponds to the large gradient of total electron density as a function of *M* shell. The density is higher than 1000 cm^{-3} at the center of the Io plasma torus (Dougherty et al., 2017), but at $M < 5.5$ the density is much lower and $f_{pe}/f_{ce} < 1$.

The whistler-mode waves at high latitudes are roughly separated at $R = 2.5$ (magenta dashed line in Figure 2b). At $R > 2.5$, the significant wave power extends to $15 < M < 30$ at |MagLat| ~45°-60°. At $R < 2.5$, the whistler-mode waves have high power near Io's orbit ($M{\sim}6$) and the major power shifts to higher latitudes with increasing *M* shell up to $M{\sim}13$. It is worth noting that the spatial extent of high-latitude waves is much smaller than the waves at low latitudes due to converging magnetic field lines.

The detailed wave spectra at different magnetic latitudes are presented in Figures 2d-f. At $|MagLat| < 25\,°$(Figure 2d), the statistical wave spectrum shows a separation between chorus ($f > 0.05f_{ce,eq}$) and hiss ($f < 0.05f_{ce,eq}$) with a wave power minimum at $0.05f_{ce,eq}$ at $M < 10$. The chorus and hiss wave powers merge at $M > 10$. At $25\,° < |MagLat| < 50\,°$(Figure 2e), the hiss wave powers are comparable to the power near the equator, while the chorus wave powers are significantly reduced. A group of whistler-mode waves are also observed at frequencies below $f_{ce,eq}$ at $M > 18$, which are probably the extension of the waves at higher latitudes. At $50\,° < |MagLat| < 70\,°$(Figure 2f), the whistler-mode waves at frequencies above 1 kHz at $M < 10$ are related to the waves produced near the Io footprint. The whistler-mode waves observed at lower frequencies (<1 kHz) may have a similar frequency range to the hiss waves originating from the equator at $M < 10$ or auroral hiss waves at the polar region. The wave powers are low at $f < 0.05\,f_{ce,eq}$ frequencies, as $f_{cp,local}$ becomes comparable or higher than $0.05f_{ce,eq}$ (Figure 1g).

Figures 1 and 2 suggest that the three major types of whistler-mode waves at $f_{cp,local} < f < f_{ce,eq}$ could be separated by spatial region and wave frequency. Hiss waves originating from the equator are mainly observed at $f < 0.05f_{ce,eq}$ frequencies over |MagLat| ~0°-50°. Chorus waves are mainly observed at $0.05\,f_{ce,eq} < f < f_{ce,eq}$ frequencies over |MagLat| ~0°-20°. High-latitude whistler-mode waves are mainly observed at $0.05\,f_{ce,eq} < f < f_{ce,eq}$ frequencies over |MagLat| ~30°-70°, and are further divided into two groups at $R = 2.5$ due to their apparently different sources. The distributions and properties for each wave type are presented in Figures 3 and 4.

The distributions of hiss wave frequency spectra for different *M* shells (Figure 3a) suggest that the hiss waves are mainly observed at frequencies below 1 kHz, with the majority of wave power located at 100-500 Hz frequencies. The RMS wave amplitude distribution (Figure 3b) suggests that the hiss waves are observed over $5.5 < M < 15$ and the average wave amplitude has a weak latitudinal dependence from 0° to 50°. The $E_w/(cB_w)$ ratio (Figure 3c) is calculated using the RMS wave magnetic and electric field amplitudes considering the effective antenna length (~2.41 m) of the Waves instrument (Kurth et al., 2017), where *c* is the speed of light. Although the ratio between plasma frequency and electron gyrofrequency (f_{pe}/f_{ce}) changes with latitude and *M* shell, we adopt the $E_w/(cB_w)$ ratio as a qualitative estimate of the wave normal angle variation (Stix, 1992). The $E_w/(cB_w)$ ratio is low ($\lesssim 0.5$) at $M > 10$ and $|MagLat| < 20\,°$, suggesting predominantly parallel propagating waves and hence the possible local wave generation source. The $E_w/(cB_w)$ ratio is lower at low latitudes than high latitudes. Although it is expected that $E_w/(cB_w)$ increases as the waves propagate to higher latitudes due to the lower f_{pe}/f_{ce} ratio, the trend of $E_w/(cB_w)$ in Figure 3c is still consistent with the scenario of wave amplification near the equator and subsequent wave propagation to high latitudes. The $E_w/(cB_w)$ ratio is lower at high *M* shells than those at low *M* shells, suggesting that the hiss waves at $M < 10$ may originate from the remote source of whistler-mode waves at $M > 10$.

The chorus wave frequency (Figure 3d) increases more rapidly with decreasing *M* shell than hiss, and the frequency of wave power spectral density follows the $f_{ce,eq}$ variation. The chorus waves are mainly observed at $5.5 < M < 13$ and $|MagLat| < 20°$, with high RMS wave amplitudes at $8 < M < 11$ and |MagLat| ~5°-15° (Figure 3e). The latitudinal distribution suggests a wave amplification process as the generated waves propagate and intensify from the equator to |MagLat|~10°, and subsequently decrease in amplitude due to a wave damping process occurring at $|MagLat| > 20°$. The suggestion of local wave generation process is supported by the statistically low $E_w/(cB_w)$ ratios ($\lesssim 0.5$) of chorus waves near the equator (Figure 3f).

The distributions and properties of high-latitude whistler-mode waves are shown in Figures 3g-i. A group of whistler-mode waves are observed at $f > 1$ kHz frequencies over the region of $R < 2.5$ and $5.5 < M < 10$. These waves are probably generated near the Io footprint and propagate with an oblique wave normal angle within the high-density region. Another group of whistler-mode waves are observed at $f < 1$ kHz frequencies over the region of $R > 2.5$ and $M > 5.5$, with major power located at $10 < M < 25$. These waves may be not locally generated but have a remote source from propagation. The main power of auroral hiss waves at high M shells ($M > 20$) and high latitudes (>60°) are not included in our survey due to $f_{cp,local} > f_{ce,eq}$. The $E_w/(cB_w)$ ratio is high ($\gtrsim 1$) for both groups of high-latitude whistler-mode waves.

Figure 4 shows the spatial distributions of wave occurrence rates for different wave amplitudes of hiss, chorus, and high-latitude whistler-mode waves. The hiss wave occurrence rates with 20-50 pT amplitudes (Figure 4a) are >10% over a broad region, and become higher at higher latitudes or near $M = 6$ possibly because of the wave power focusing into a small spatial region after propagating from the equatorial source. The occurrence rates for higher amplitude waves are significantly reduced at high latitudes (Figures 4b-c), and the waves with >100 pT amplitudes are observed mainly within 20° of the equator (Figure 4c). The chorus wave occurrence rates (Figures 4d-f) are comparable to those of hiss at $|MagLat| < 20°$. Chorus waves with >100 pT amplitudes are mostly observed in the region of $8 < M < 12$ and $|MagLat| < 16°$ (Figure 4f). The distributions of large amplitude waves suggest that the energy source of chorus and hiss from energetic electrons is within 20° from the equator. Figure 4g shows that the peak occurrence rates of the two high-latitude wave groups with 20-50 pT are higher than 10%. The wave occurrence rates with >50 pT amplitude are much lower than those of chorus or hiss (Figure 4h), and the waves with >100 pT amplitude are rarely observed (Figure 4i).

4. Conclusions and Discussions

We conducted a statistical survey of the whistler-mode wave amplitude distributions and frequency spectra for the waves at $f_{cp,local} < f < f_{ce,eq}$ frequencies using the Juno Waves data from 2016 to 2023. The electromagnetic waves in this frequency range include chorus and hiss waves observed at 0°-50° latitudes which originate from the magnetic equator, and high-latitude (>50°) whistler-mode waves, which may have multiple possible sources. Our paper presents the first study on the distributions and properties of these waves separately in Jupiter's magnetosphere. The main results are summarized below.

- Chorus waves at $0.05f_{ce,eq} < f < f_{ce,eq}$ are observed mainly over $5.5 < M < 13$ and 0°-20° latitudes, and high-amplitude (>50 pT) waves are observed over $8 < M < 12$ and 4°-16° latitudes. Their wave normal angles are seen to be mainly field-aligned. The statistical distributions suggest that chorus waves may be generated from anisotropic electrons near the equator, amplified while propagating a few degrees away from the equator, and damped at >20° latitudes.
- Hiss waves at $f_{cp,local} < f < 0.05f_{ce,eq}$ are observed over $5.5 < M < 15$ and 0°-50° latitudes. While the waves with modest amplitudes (<50 pT) have higher occurrence rates at

higher latitudes, the large amplitude (>100 pT) waves are observed only within 20° of the equator. The $E_w/(cB_w)$ ratio is lower at lower latitudes compared to that at higher latitudes, and lower at higher M shell than that at lower M shell. Hiss waves at high M shells near the equator may be locally generated or amplified by anisotropic energetic electrons. The generated chorus and hiss waves may propagate to lower altitudes and contribute to the hiss wave power at low M shells or high latitudes.

- High-latitude whistler-mode waves are mostly observed at $0.05f_{ce,eq} < f < f_{ce,eq}$ frequencies and 30°-70° latitudes with wave amplitudes below 50 pT. The high-latitude whistler-mode waves are comprised of two groups: one with frequencies above 1 kHz over the region of $R < 2.5$ and $5.5 < M < 10$, and another with frequencies below 1 kHz over the region of $R > 2.5$ and $M > 10$. The waves at $R < 2.5$ may be generated near the Io footprint, and the waves at $R > 2.5$ may have a source from the propagation effects. Both wave groups may propagate from their source with oblique wave normal angles.

Although the chorus and hiss waves are observed in similar regions in Jupiter's magnetosphere, their statistical distributions and properties need to be resolved separately because of the different roles they play in radiation belt electron acceleration and precipitation (Ma et al., 2020; Ni et al., 2018). Both typical wave events and statistical distributions demonstrate that the chorus and hiss have different spatial coverage and propagation properties, suggesting their different sources. The wave power separation between chorus and hiss at $0.05f_{ce,eq}$ is evident at $M < 10$. Due to their different wave frequencies, the wave phase velocities of chorus and hiss are different, which determines the energy of electron precipitation and acceleration during resonant wave-particle interactions. Our dataset also reveals the distributions of two groups of high-latitude whistler-mode waves which may cause additional electron precipitation. The Landau resonance of electrons by oblique waves at high latitudes may contribute to the <10 keV electron precipitation, in addition to the higher energy electron scattering by whistler-mode waves near the equator as reported by Li et al. (2021). In addition, the local field-aligned density ducts could provide an efficient channel for energetic electron precipitation (e.g., Kang et al., 2024). The statistical distributions of whistler-mode waves in our study could be valuable for future modeling of energetic electron flux distribution and dynamic evolution of Jupiter's outer radiation belt.

Acknowledgments

We would like to acknowledge the NASA subcontract 699046X to UCLA and subcontract Q99064JAR to Boston University under prime contract ZZM06AA75C. This work was supported by the NASA grants 80NSSC20K0196, 80NSSC20K0557, and 80NSSC24K0572, and the NSF grants AGS-2225445 and AGS-2402179. The research conducted at the University of Iowa was supported by NASA through contract 699041X with the Southwest Research Institute. WSK acknowledges the use of the Space Physics Data Repository at the University of Iowa supported by the Roy J. Carver Charitable Trust.

Open Research

The Juno data are retrieved from NASA Planetary Data System (https://pds-ppi.igpp.ucla.edu/mission/JUNO). This study uses the Juno Waves survey mode data (*Kurth and*

Piker, 2022). The survey results in this study are available at the data repository (*Ma et al.*, 2024b).

References

Agapitov, O., A. Artemyev, V. Krasnoselskikh, Y. V. Khotyaintsev, D. Mourenas, H. Breuillard, M. Balikhin, and G. Rolland (2013), Statistics of whistler-mode waves in the outer radiation belt: Cluster STAFF-SA measurements, J. Geophys. Res. Space Physics, 118, 3407–3420, doi:10.1002/jgra.50312.

Bagenal, F., A. Adriani, F. Allegrini, S. J. Bolton, B. Bonfond, E. J. Bunce, J. E. P. Connerney, S. W. H. Cowley, R. W. Ebert, G. R. Gladstone, C. J. Hansen, W. S. Kurth, S. M. Levin, B. H. Mauk, D. J. McComas, C. P. Paranicas, D. Santos-Costa, R. M. Thorne, P. Valek, J. H. Waite, and P. Zarka (2017), Magnetospheric Science Objectives of the Juno Mission, Space Sci. Rev., 213, 219-287, doi:10.1007/s11214-014-0036-8.

Bhattacharya, B., Thorne, R. M., Williams, D. J., Khurana, K. K., & Gurnett, D. A. (2005). Diffuse auroral precipitation in the Jovian upper atmosphere and magnetospheric electron flux variability. Icarus, 178(2), 406-416. https://doi.org/10.1016/j.icarus.2005.06.013

Blum, L., & Breneman, A. (2020). Observations of radiation belt losses due to cyclotron wave-particle interactions. In The dynamic loss of Earth's radiation belts (pp. 49–98). Elsevier. https://doi.org/10.1016/B978-0-12-813371-2.00003-2

Bolton, S. J., and Juno Science Team (2010), The Juno mission, Proc. Int. Astron. Union, 6 (S269), doi:10.1017/S1743921310007313.

Chen, L., W. Li, J. Bortnik, and R. M. Thorne (2012), Amplification of whistler-mode hiss inside the plasmasphere, Geophys. Res. Lett., 39, L08111, doi:10.1029/2012GL051488.

Clark, G., Mauk, B. H., Kollmann, P., Szalay, J. R., Sulaiman, A. H., Gershman, D. J., et al. (2020). Energetic proton acceleration associated with Io's footprint tail. Geophys. Res. Lett. 47 (24), e2020GL090839. doi:10.1029/2020gl090839

Clark, G., J. R. Szalay, A. H. Sulaiman, J. Saur, P. Kollmann, B. H. Mauk, C. Paranicas, V. Hue, T. Greathouse, F. Allegrini, A. Glocer, K. Garcia-Sage, and S. Bolton (2023), Energetic proton acceleration by EMIC waves in Io's footprint tail, Front. Astron. Space Sci., 10:1016345, doi:10.3389/fspas.2023.1016345.

Connerney, J. E. P., M. Benn, J. B. Bjarno, et al. (2017), The Juno Magnetic Field Investigation. Space Sci Rev 213, 39-138, https://doi.org/10.1007/s11214-017-0334-z.

Connerney, J. E. P., Timmins, S., Herceg, M., & Joergensen, J. L. (2020). A Jovian magnetodisc model for the Juno era. Journal of Geophysical Research: Space Physics, 125, e2020JA028138. https://doi.org/10.1029/2020JA028138

Connerney, J. E. P., Timmins, S., Oliversen, R. J., Espley, J. R., Joergensen, J. L., Kotsiaros, S., et al. (2022a). A new model of Jupiter's magnetic field at the completion of Juno's Prime Mission. Journal of Geophysical Research: Planets, 127, e2021JE007055. https://doi.org/10.1029/2021JE007055

Connerney, J. E. P. (2022b), Juno MAG CALIBRATED DATA J V1.0, JNO-J-3-FGM-CAL-V1.0 [Dataset], NASA Planetary Data System, https://doi.org/10.17189/1519711.

Dougherty, L. P., Bodisch, K. M., and Bagenal, F. (2017), Survey of Voyager plasma science ions at Jupiter: 2. Heavy ions, J. Geophys. Res. Space Physics, 122, 8257- 8276, doi:10.1002/2017JA024053.

Elliott, S. S., Gurnett, D. A., Yoon, P. H., Kurth, W. S., Mauk, B. H., Ebert, R. W., et al. (2020). The generation of upward-propagating whistler mode waves by electron beams in the Jovian polar regions. Journal of Geophysical Research: Space Physics, 125, e2020JA027868. https://doi.org/10.1029/2020JA027868.

Horne, R. B., R. M. Thorne, S. A. Glauert, J. D. Menietti, Y. Y. Shprits, and D. A. Gurnett (2008), Gyro-resonant electron acceleration at Jupiter, Nature Physics, 4, 301-304, doi:10.1038/nphys897.

Kang, N., Artemyev, A. V., Bortnik, J., Zhang, X.-J., & Angelopoulos, V. (2024). The Principal role of chorus ducting for night-side relativistic electron precipitation. Geophysical Research Letters, 51, e2024GL110365. https://doi.org/10.1029/2024GL110365

Kurth, W. S., G. B. Hospodarsky, D. L. Kirchner, B. T. Mokrzycki, T. F. Averkamp, W. T. Robison, C. W. Piker, M. Sampl, and P. Zarka (2017), The Juno Waves Investigation, Space Sci. Rev., 213, 1-4, 347-392, doi:10.1007/s11214-017-0396-y.

Kurth, W. S., and Piker C. W. (2022), JUNO E/J/S/SS WAVES CALIBRATED SURVEY FULL RESOLUTION V2.0, JNO-E/J/SS-WAV-3-CDR-SRVFULL-V2.0 [Dataset], NASA Planetary Data System, doi:10.17189/1520498.

Li, W., R. M. Thorne, V. Angelopoulos, J. Bortnik, C. M. Cully, B. Ni, O. LeContel, A. Roux, U. Auster, and W. Magnes (2009), Global distribution of whistler-mode chorus waves observed on the THEMIS spacecraft, Geophys. Res. Lett., 36, L09104, doi:10.1029/2009GL037595.

Li, W., R. M. Thorne, J. Bortnik, Y. Y. Shprits, Y. Nishimura, V. Angelopoulos, C. Chaston, O. Le Contel, and J. W. Bonnell (2011), Typical properties of rising and falling tone chorus waves, Geophys. Res. Lett., 38, L14103, doi:10.1029/2011GL047925.

Li, W., Q. Ma, R. M. Thorne, J. Bortnik, C. A. Kletzing, W. S. Kurth, G. B. Hospodarsky, and Y. Nishimura (2015), Statistical properties of plasmaspheric hiss derived from Van Allen Probes data and their effects on radiation belt electron dynamics. J. Geophys. Res. Space Physics, 120, 3393-3405. doi: 10.1002/2015JA021048.

Li, W., O. Santolík, J. Bortnik, R. M. Thorne, C. A. Kletzing, W. S. Kurth, and G. B. Hospodarsky (2016), New chorus wave properties near the equator from Van Allen Probes wave observations, Geophys. Res. Lett., 43, 4725–4735, doi:10.1002/2016GL068780.

Li, W., Shen, X.-C., Menietti, J. D., Ma, Q., Zhang, X.-J., Kurth, W. S., & Hospodarsky, G. B. (2020). Global Distribution of Whistler Mode Waves in Jovian Inner Magnetosphere. Geophysical Research Letters, 47, e2020GL088198. https://doi.org/10.1029/2020GL088198.

Li, W., Ma, Q., Shen, X.-C., Zhang, X.-J., Mauk, B. H., Clark, G., et al. (2021). Quantification of diffuse auroral electron precipitation driven by whistler mode waves at Jupiter. Geophysical Research Letters, 48, e2021GL095457. https://doi.org/10.1029/2021GL095457.

Lorentzen, K. R., J. B. Blake, U. S. Inan, and J. Bortnik (2001), Observations of relativistic electron microbursts in association with VLF chorus, J. Geophys. Res., 106(A4), 6017–6027, doi:10.1029/2000JA003018.

Ma, Q., et al. (2016), Characteristic energy range of electron scattering due to plasmaspheric hiss, J. Geophys. Res. Space Physics, 121, 11,737–11,749, doi:10.1002/2016JA023311.

Ma, Q., Li, W., Zhang, X.-J., Bagenal, F. (2020). Energetic electron scattering due to whistler mode chorus waves using realistic magnetic field and density models in Jupiter's magnetosphere. Journal of Geophysical Research: Space Physics, 125, e2020JA027968. https://doi.org/10.1029/2020JA027968

Ma, Q., Li, W., Zhang, X.-J., Shen, X.-C., Daly, A., Bortnik, J., et al. (2021). Energetic electron distributions near the magnetic equator in the Jovian plasma sheet and outer radiation belt using Juno observations. Geophysical Research Letters, 48, e2021GL095833. https://doi.org/10.1029/2021GL095833

Ma, Q., X. Chu, D. Ma, S. Huang, W. Li, J. Bortnik, and X.-C. Shen (2023), Evaluating the performance of empirical models of total electron density and whistler-mode wave amplitude in the Earth's inner magnetosphere, Front. Astron. Space Sci., 10:1232702, doi: 10.3389/fspas.2023.1232702.

Ma, Q., Li, W., Zhang, X.-J., Bortnik, J., Shen, X.-C., Daly, A., et al. (2024a). Generation and impacts of whistler-mode waves during energetic electron injections in Jupiter's outer radiation belt. Journal of Geophysical Research: Space Physics, 129, e2024JA032624. https://doi.org/10.1029/2024JA032624

Ma, Q., W. Li, X.-J. Zhang, N. Kang, J. Bortnik, M. Qin, et al. (2024b), Dataset for "Survey of Whistler-mode Wave Amplitudes and Frequency Spectra in Jupiter's Magnetosphere". [Dataset], figshare, https://doi.org/10.6084/m9.figshare.26198681.

Mauk, B. H., Williams, D. J., McEntire, R. W., Khurana, K. K., and Roederer, J. G. (1999), Storm-like dynamics of Jupiter's inner and middle magnetosphere, J. Geophys. Res., 104(A10), 22759- 22778, doi:10.1029/1999JA900097.

Menietti, J. D., Groene, J. B., Averkamp, T. F., Horne, R. B., Woodfield, E. E., Shprits, Y. Y., de Soria-Santacruz Pich, M., and Gurnett, D. A. (2016), Survey of whistler mode chorus intensity at Jupiter, J. Geophys. Res. Space Physics, 121, 9758- 9770, doi:10.1002/2016JA022969.

Menietti, J. D., Averkamp, T. F., Imai, M., Kurth, W. S., Clark, G. B., Allegrini, F., et al. (2020). Low-latitude whistler-mode and higher-latitude Z-mode emission at Jupiter observed by Juno. Journal of Geophysical Research: Space Physics, 126, e2020JA028742. https://doi.org/10.1029/2020JA028742

Menietti, J. D., Averkamp, T. F., Kurth, W. S., Imai, M., Faden, J. B., Hospodarsky, G. B., et al. (2021). Analysis of whistler-mode and Z-mode emission in the Juno primary mission. Journal of Geophysical Research: Space Physics, 126, e2021JA029885. https://doi.org/10.1029/2021JA029885

Menietti, J. D., Averkamp, T. F., Kurth, W. S., Faden, J. B., & Bolton, S. J. (2023). Survey and analysis of whistler- and Z-mode emission in the Juno extended mission. Journal of

Geophysical Research: Space Physics, 128, e2023JA032037. https://doi.org/10.1029/2023JA032037

Meredith, N. P., R. B. Horne, A. Sicard-Piet, D. Boscher, K. H. Yearby, W. Li, and R. M. Thorne (2012), Global model of lower band and upper band chorus from multiple satellite observations, J. Geophys. Res., 117, A10225, doi:10.1029/2012JA017978.

Ni, B. B., Huang, J., Ge, Y. S., Cui, J., Wei, Y., Gu, X. D., Fu, S., Xiang, Z., and Zhao, Z. Y. (2018). Radiation belt electron scattering by whistler-mode chorus in the Jovian magnetosphere: Importance of ambient and wave parameters. Earth Planet. Phys., 2, 1–14. http://doi.org/10.26464/epp2018001

Santolík, O., D. A. Gurnett (2002), Propagation of auroral hiss at high altitudes, Geophys. Res. Lett., 29(10), doi:10.1029/2001GL013666.

Santolík, O., D. A. Gurnett, J. S. Pickett, M. Parrot, and N. Cornilleau-Wehrlin (2003), Spatio-temporal structure of storm-time chorus, J. Geophys. Res., 108, 1278, doi:10.1029/2002JA009791, A7.

Shprits, Y. Y., Menietti, J. D., Gu, X., Kim, K. C., and Horne, R. B. (2012), Gyroresonant interactions between the radiation belt electrons and whistler mode chorus waves in the radiation environments of Earth, Jupiter, and Saturn: A comparative study, J. Geophys. Res., 117, A11216, doi:10.1029/2012JA018031.

Stix, T. H. (1992). Waves in plasmas, American Institute of Physics, ISBN 0883188597

Sulaiman, A. H., Hospodarsky, G. B., Elliott, S. S., Kurth, W. S., Gurnett, D. A., Imai, M., et al. (2020). Wave-particle interactions associated with Io's auroral footprint: Evidence of Alfvén, ion cyclotron, and whistler modes. Geophys. Res. Lett. 47, e2020GL088432. doi:10.1029/2020gl088432

Sulaiman, A. H., Mauk, B. H., Szalay, J. R., Allegrini, F., Clark, G., Gladstone, G. R., et al. (2022). Jupiter's low-altitude auroral zones: Fields, particles, plasma waves, and density depletions. Journal of Geophysical Research: Space Physics, 127, e2022JA030334. https://doi. org/10.1029/2022JA030334

Szalay, J. R., Allegrini, F., Bagenal, F., Bolton, S. J., Bonfond, B., Clark, G., et al. (2020). A new framework to explain changes in Io's footprint tail electron fluxes. Geophys. Res. Lett. 47 (18), e2020GL089267. doi:10.1029/2020gl089267

Thorne, R. M., B. Ni, X. Tao, R. B. Horne, and N. P. Meredith (2010), Scattering by chorus waves as the dominant cause of diffuse auroral precipitation, Nature, 467, 943–946, doi:10.1038/nature09467.

Thorne, R. M., W. Li, B. Ni, Q. Ma, J. Bortnik, L. Chen, D. N. Baker, H. E. Spence, G. D. Reeves, M. G. Henderson, C. A. Kletzing, W. S. Kurth, G. B. Hospodarsky, J. B. Blake, J. F. Fennell, S. G. Claudepierre, and S. G. Kanekal (2013), Rapid local acceleration of relativistic radiation-belt electrons by magnetospheric chorus, Nature, 504, 411-414, doi:10.1038/nature12889.

Tomás, A. T., J. Woch, N. Krupp, A. Lagg, K.-H. Glassmeier, and W. S. Kurth (2004), Energetic electrons in the inner part of the Jovian magnetosphere and their relation to auroral emissions, J. Geophys. Res., 109, A06203, doi:10.1029/2004JA010405.

Wang, K., R. M. Thorne, and R. B. Horne (2008), Origin of Jovian hiss in the extended Io torus, Geophys. Res. Lett., 35, L16105, doi:10.1029/2008GL034636.

Woodfield, E. E., R. B. Horne, S. A. Glauert, J.D. Menietti, and Y. Y. Shprits (2013), Electron acceleration at Jupiter: input from cyclotron-resonant interaction with whistler-mode chorus waves, Ann. Geophys., 31, 1619-1630, doi:10.5194/angeo-31-1619-2013.

Woodfield, E. E., Horne, R. B., Glauert, S. A., Menietti, J. D., and Shprits, Y. Y. (2014), The origin of Jupiter's outer radiation belt, J. Geophys. Res. Space Physics, 119, 3490- 3502, doi:10.1002/2014JA019891.

Xiao, F., Thorne, R. M., Gurnett, D. A., and Williams, D. J. (2003), Whistler-mode excitation and electron scattering during an interchange event near Io, Geophys. Res. Lett., 30, 1749, doi:10.1029/2003GL017123, 14.

Figures and Captions

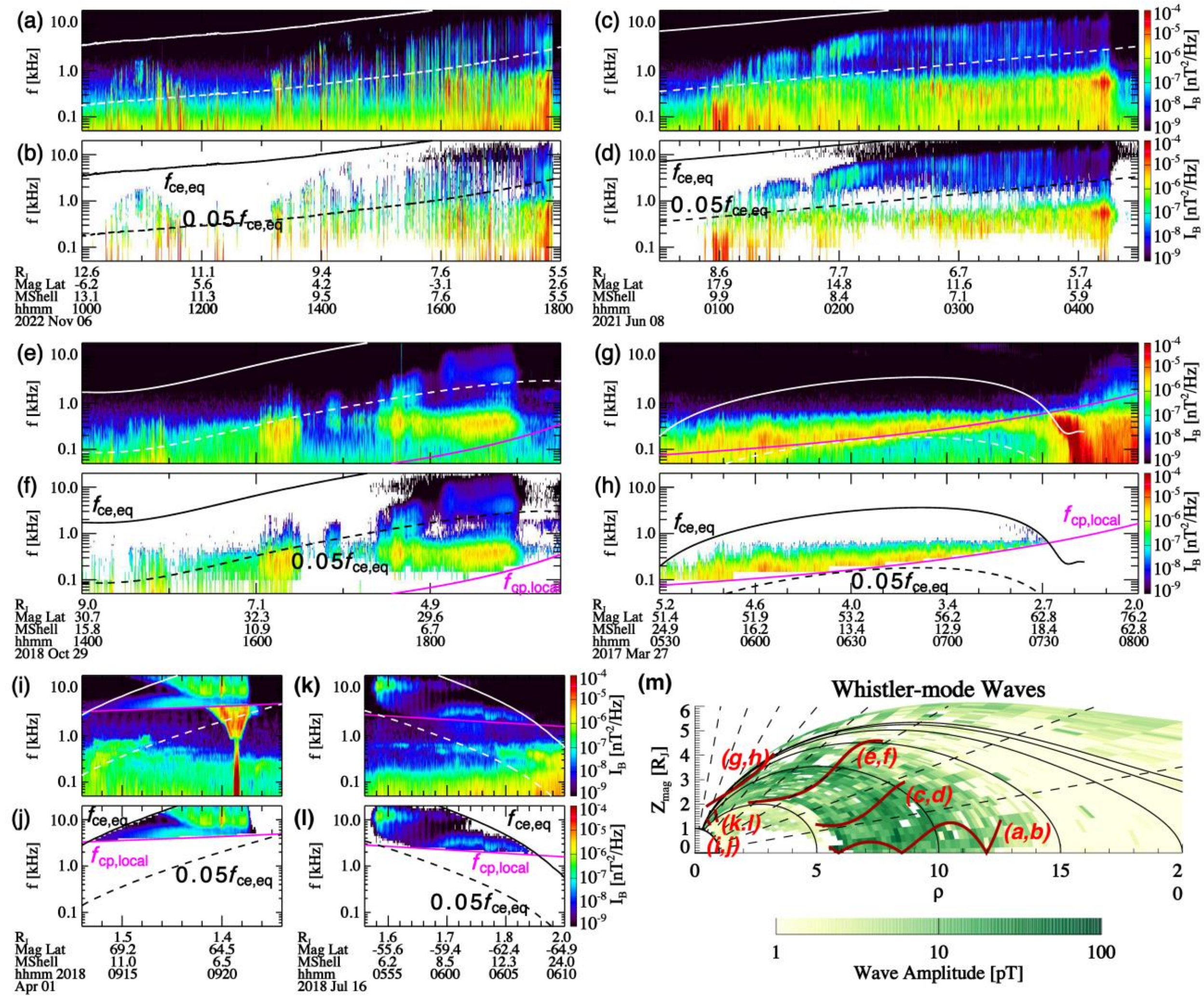

Figure 1. Examples of different types of whistler-mode waves observed at different locations by Juno. (a) Wave magnetic field power spectrogram at 50 Hz – 20 kHz frequencies measured by the Waves instrument at |MagLat| ~0°-10°; (b) selected whistler-mode waves; (c-l) same as (a-b) but observed during the events at MagLat ~10°-20°, MagLat ~20°-40°, MagLat >50° and $R > 2.5$, MagLat >50° and $R < 1.5$, and |MagLat| >50° and $1.5 < R < 2$, respectively. In the upper (or lower) panels of each event, the white (or black) solid, magnenta solid, and white (or black) dashed lines are $f_{ce,eq}$, $f_{cp,local}$, and 0.05 $f_{ce,eq}$ frequencies, respectively. (m) RMS magnetic amplitudes of whistler-mode waves, overplotted with the Juno trajectories during the events displayed in panels (a-l).

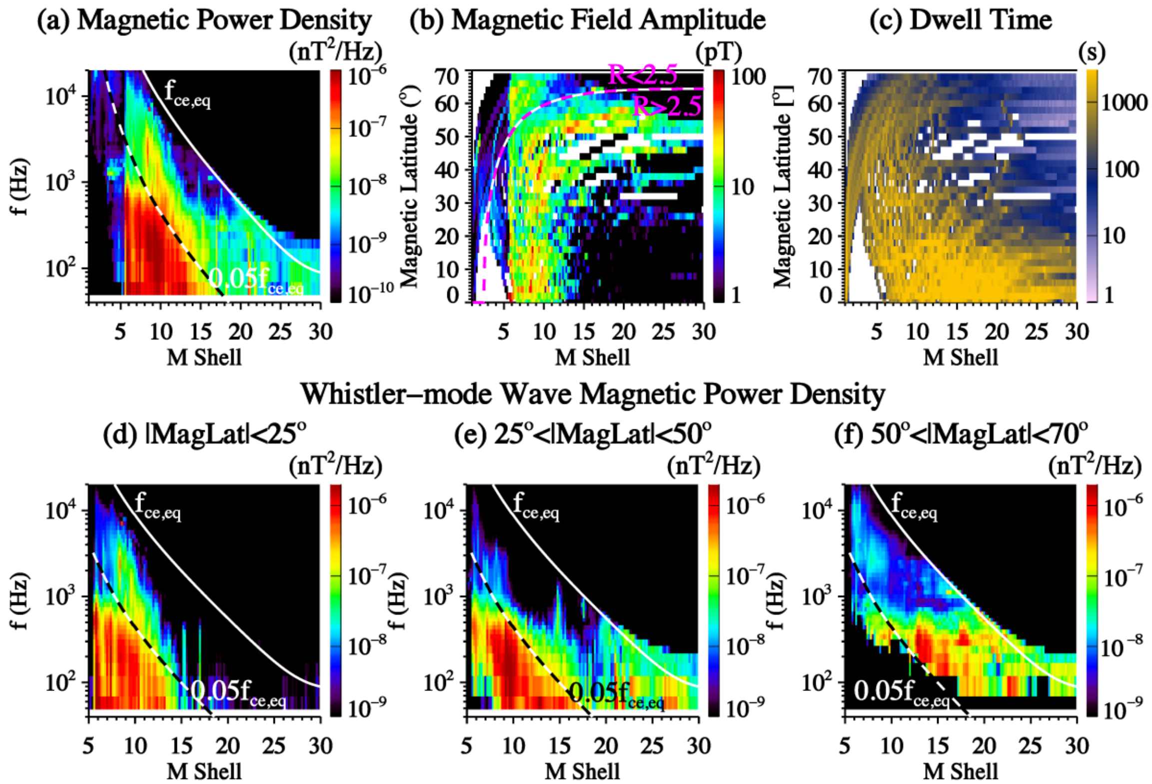

Figure 2. Statistical distribution of whistler-mode wave frequency spectra and wave amplitude distributions. (a) Average power spectral densities of whistler-mode waves at 50 Hz – 20 kHz frequencies at $M < 30$; (b) RMS wave amplitude distribution of whistler-mode waves over $f_{cp,local} < f < f_{ce,eq}$ frequencies as a function of *M* shell and |MagLat|; (c) data sampling distribution; (d-f) same as panel (a) but for different latitudinal ranges. The white solid and white-black dashed lines in (a, d, e, f) are $f_{ce,eq}$ and 0.05 $f_{ce,eq}$ frequencies from JRM33 and CON2020 magnetic field models. The white-magneta dashed line in (b) is the $R = 2.5$ line.

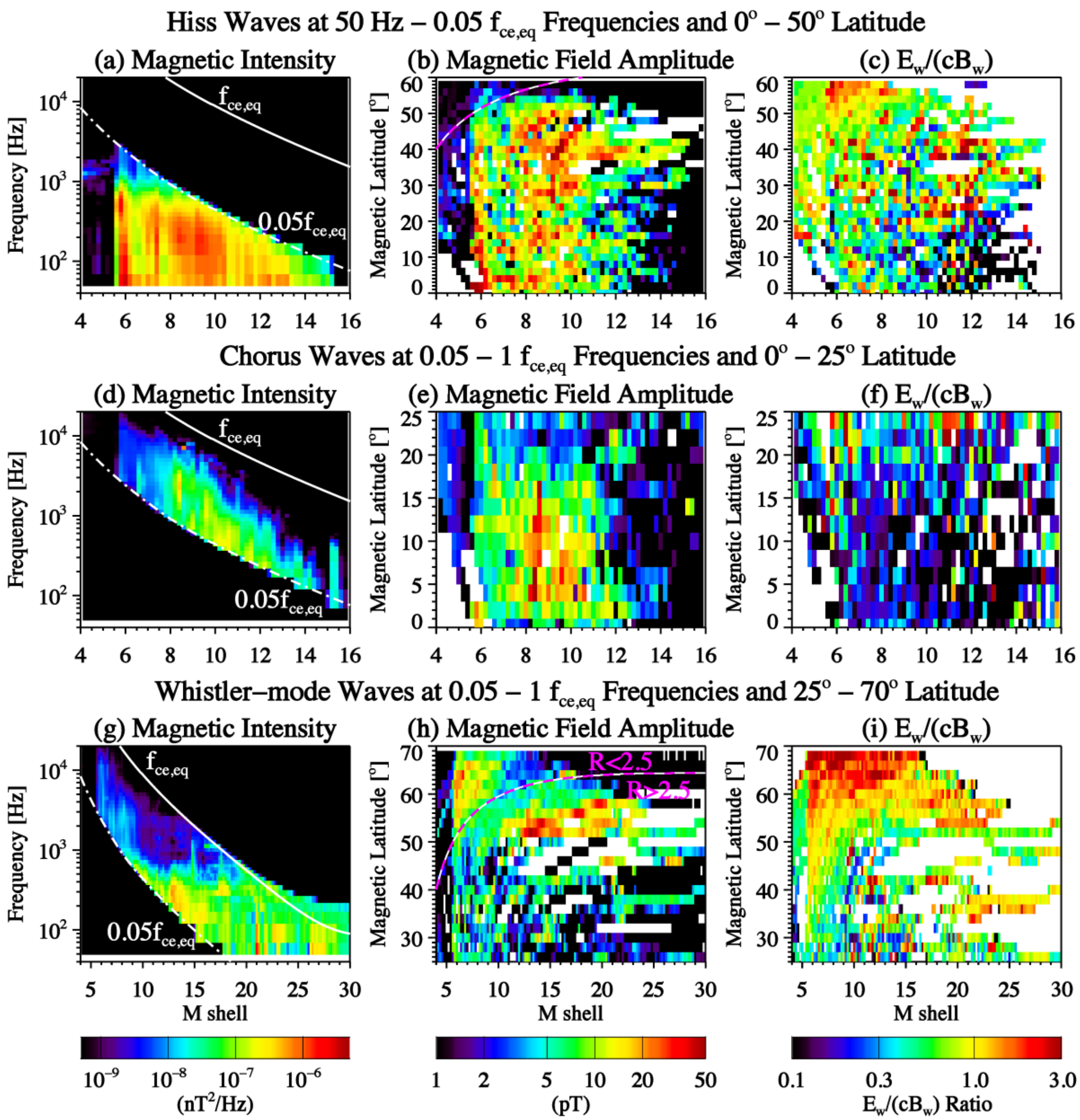

Figure 3. Statistical distributions of hiss, chorus, and high-latitude whistler-mode wave frequency spectra and amplitudes. (a) Average wave power spectral densities as a function of frequency and *M* shell, (b) RMS wave amplitudes as a function of |MagLat| and M shell, and (c) wave electric to magnetic field amplitude ratio (E_w/cB_w) of hiss waves at 50 Hz – 0.05 $f_{ce,eq}$ frequencies and |MagLat| ~0°-50°; (d-f) same as (a-c) but for chorus waves at $0.05 – 0.5f_{ce,eq}$ frequencies and |MagLat| ~0°-25°; (g-i) same as (a-c) but for high-latitude whistler-mode waves at $0.05f_{ce,eq} – f_{ce,eq}$ frequencies.

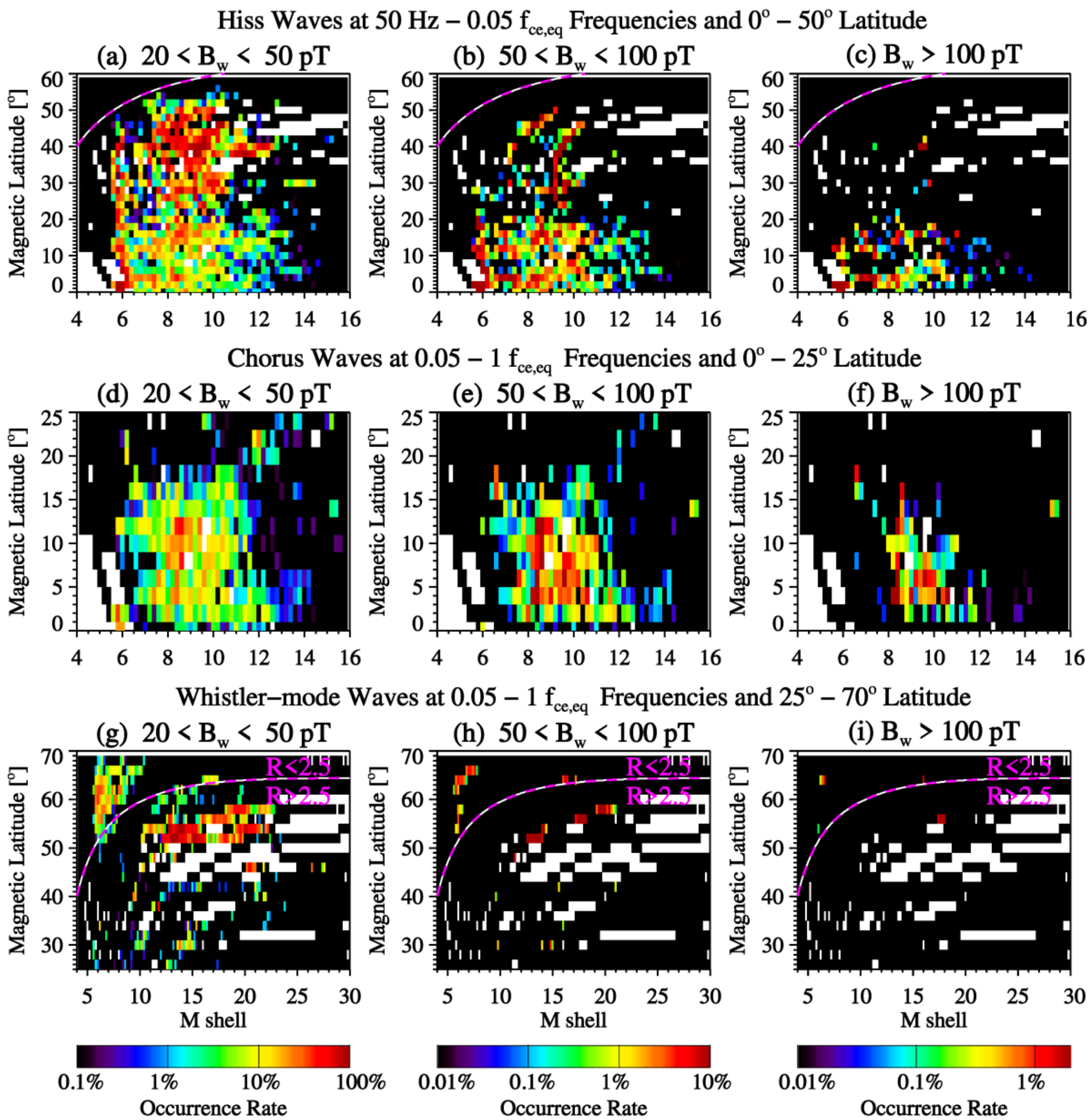

Figure 4. Amplitude occurrence rate distributions of hiss, chorus, and high-latitude whistler-mode waves. (a-c) Occurrence rates of hiss waves with amplitudes of 20–50 pT, 50–100 pT, and >100 pT, respectively. (d-f) Same as (a-c) but for chorus waves. (g-i) Same as (a-c) but for high-latitude whistler-mode waves at $0.05f_{ce,eq}-f_{ce,eq}$ frequencies. The white-magneta dashed lines in the top and bottom rows represent $R = 2.5$.

Figure 1.

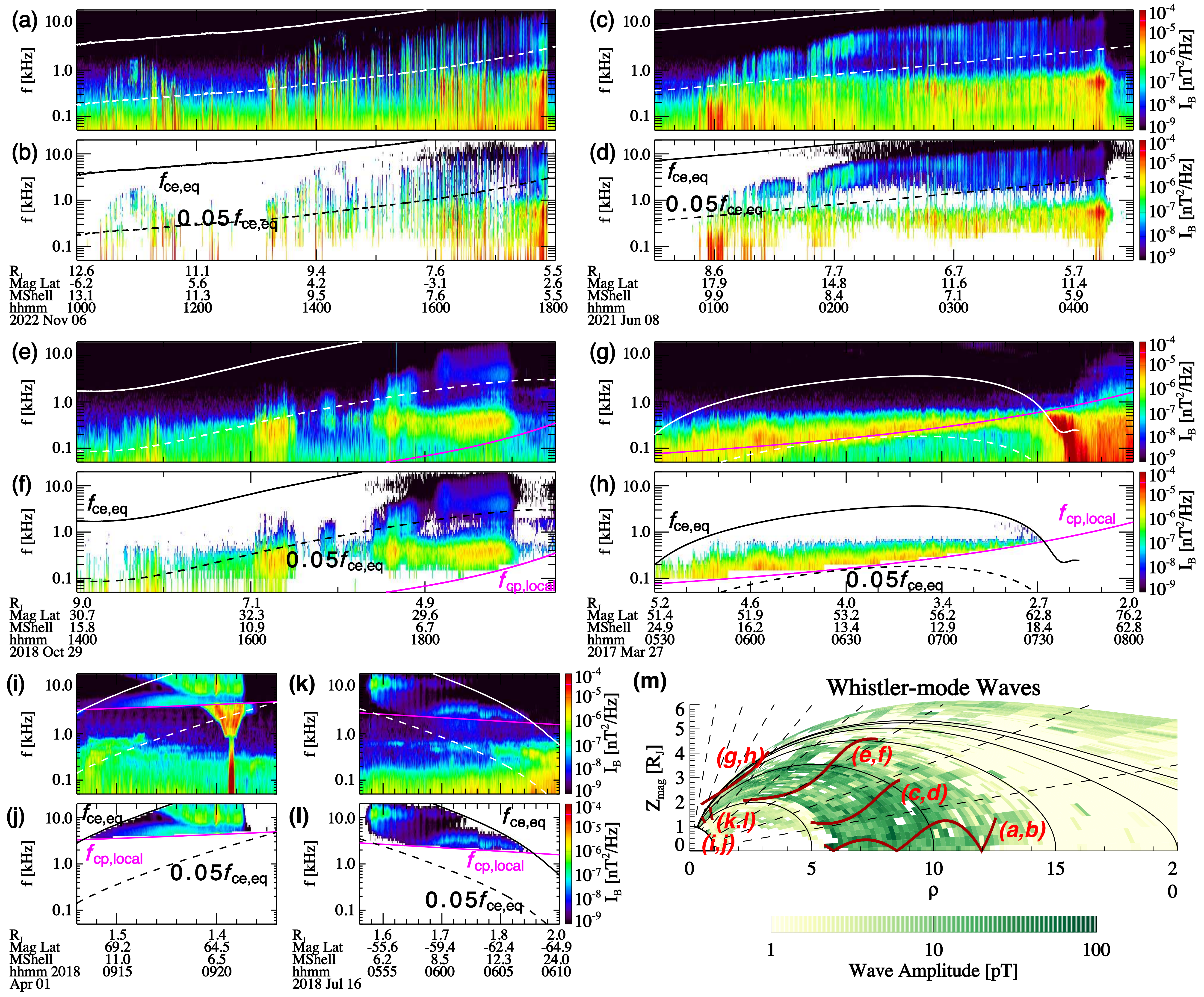

(a)
(b)
(c)
(d)
(e)
(f)
(g)
(h)
(i)
(j)
(k)
(l)
(m)
f [kHz]
I_B [nT^2/Hz]
f_ce,eq
0.05f_ce,eq
f_cp,local
R_J
Mag Lat
MShell
hhmm
2022 Nov 06
2021 Jun 08
2018 Oct 29
2017 Mar 27
hhmm 2018 Apr 01
2018 Jul 16
Whistler-mode Waves
Z_mag [R_J]
ρ
Wave Amplitude [pT]
(a,b)
(c,d)
(e,f)
(g,h)
(k,l)
(i,j)

Figure 2.

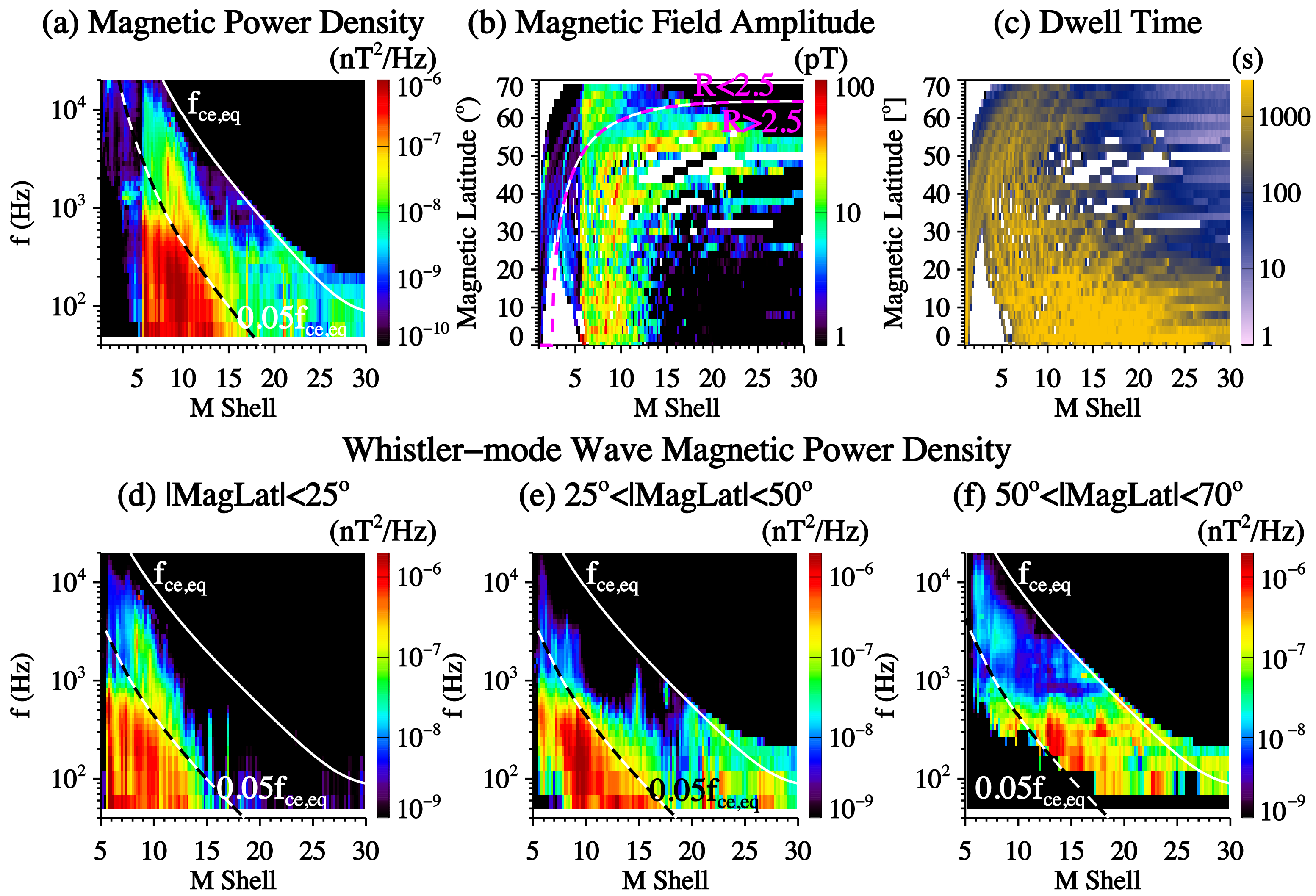
(a) Magnetic Power Density
(nT²/Hz)
f (Hz)
M Shell
f_ce,eq
0.05f_ce,eq
(b) Magnetic Field Amplitude
(pT)
Magnetic Latitude (°)
R<2.5
R>2.5
(c) Dwell Time
(s)
Magnetic Latitude [°]
Whistler–mode Wave Magnetic Power Density
(d) |MagLat|<25°
(e) 25°<|MagLat|<50°
(f) 50°<|MagLat|<70°

Figure 3.

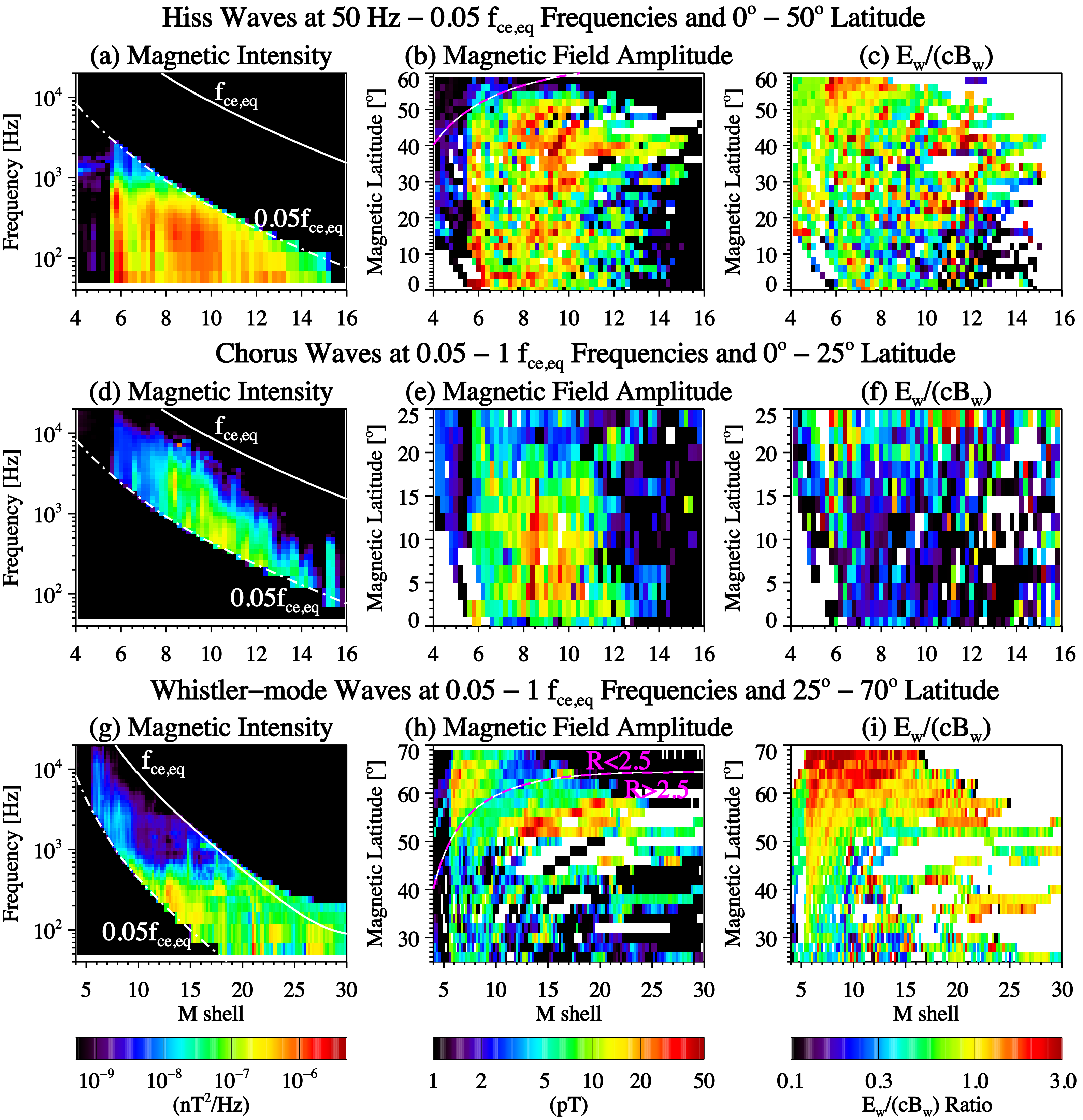

Hiss Waves at 50 Hz – 0.05 $f_{ce,eq}$ Frequencies and 0° – 50° Latitude
(a) Magnetic Intensity
(b) Magnetic Field Amplitude
(c) $E_w/(cB_w)$
Frequency [Hz]
Magnetic Latitude [°]
$f_{ce,eq}$
$0.05f_{ce,eq}$
Chorus Waves at 0.05 – 1 $f_{ce,eq}$ Frequencies and 0° – 25° Latitude
(d) Magnetic Intensity
(e) Magnetic Field Amplitude
(f) $E_w/(cB_w)$
Whistler–mode Waves at 0.05 – 1 $f_{ce,eq}$ Frequencies and 25° – 70° Latitude
(g) Magnetic Intensity
(h) Magnetic Field Amplitude
(i) $E_w/(cB_w)$
R<2.5
R>2.5
M shell
(nT^2/Hz)
(pT)
$E_w/(cB_w)$ Ratio

Figure 4.

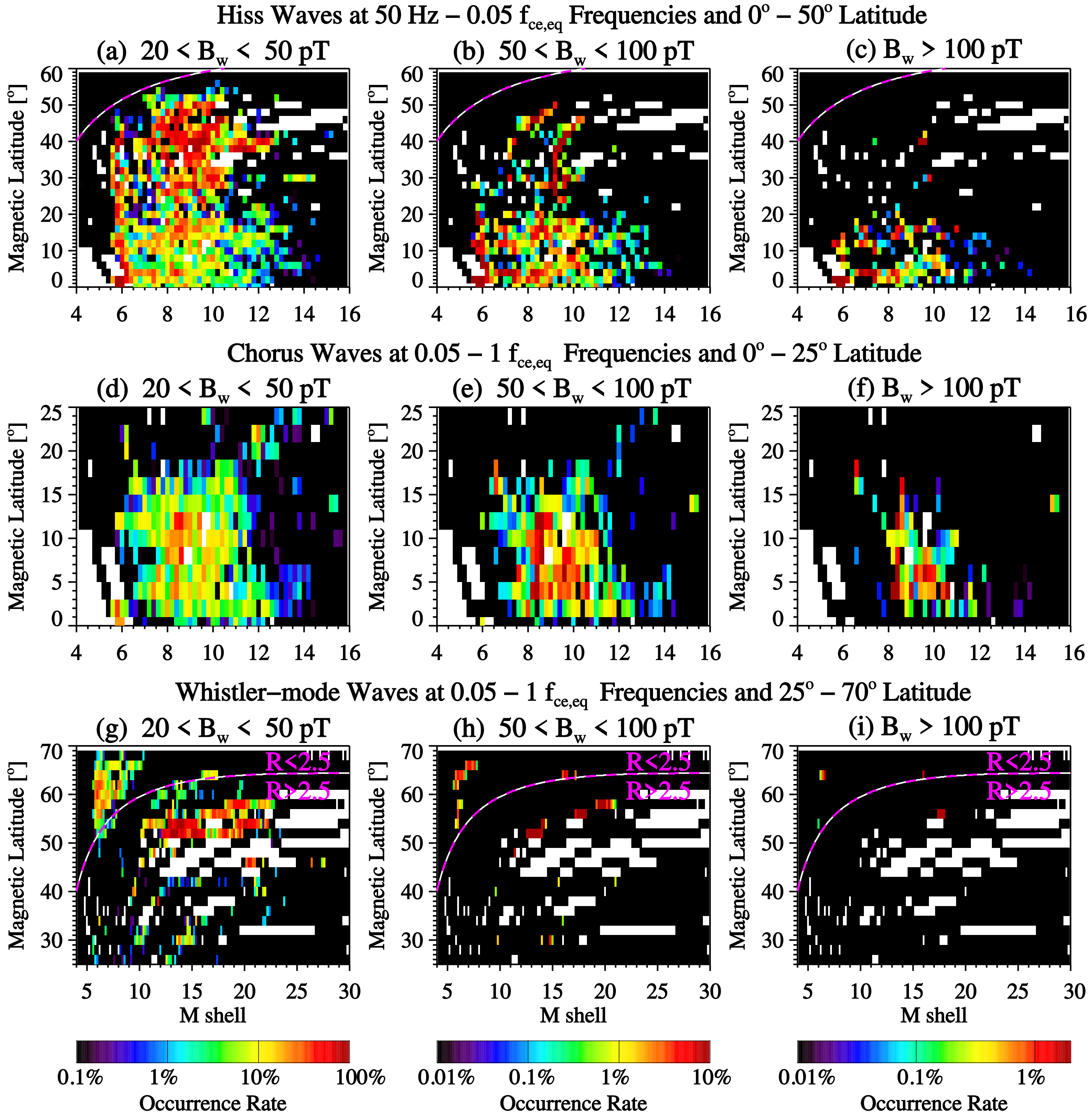

Hiss Waves at 50 Hz – 0.05 $f_{ce,eq}$ Frequencies and 0° – 50° Latitude
(a) 20 < B_w < 50 pT
(b) 50 < B_w < 100 pT
(c) B_w > 100 pT
Chorus Waves at 0.05 – 1 $f_{ce,eq}$ Frequencies and 0° – 25° Latitude
(d) 20 < B_w < 50 pT
(e) 50 < B_w < 100 pT
(f) B_w > 100 pT
Whistler–mode Waves at 0.05 – 1 $f_{ce,eq}$ Frequencies and 25° – 70° Latitude
(g) 20 < B_w < 50 pT
(h) 50 < B_w < 100 pT
(i) B_w > 100 pT
Magnetic Latitude [°]
M shell
R<2.5
R>2.5
0.1%
1%
10%
100%
0.01%
0.1%
1%
10%
0.01%
0.1%
1%
Occurrence Rate